A global Curie depth model utilising the equivalent source magnetic dipole method

Article *in* Physics of The Earth and Planetary Interiors · February 2021

DOI: 10.1016/j.pepi.2021.106672

2 authors:

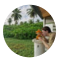

Matthew Gard
Geoscience Australia

Derrick Hasterok
University of Adelaide

A global Curie depth model utilising the equivalent source magnetic dipole method

M. Gard[a,b,*], D. Hasterok[a,c]

[a]*Department of Earth Sciences, University of Adelaide, SA, Australia*
[b]*Geoscience Australia, Canberra, ACT, Australia*
[c]*Mawson Geoscience Centre, University of Adelaide, SA, Australia*

Abstract

The depth to the Curie isotherm provides a snapshot into the deep thermal conditions of the crust, which helps constrain models of thermally controlled physical properties and processes. In this study, we present an updated global Curie depth model by employing the equivalent source dipole method to fit the lithospheric magnetic field model LCS-1 from spherical harmonic degree 16 to 100. In addition to the new field mode, we utilize all three vector components and include a laterally variable magnetic susceptibility model. We also employ an improved thermal model, TC1, to supplement the degree 1 to 15 components that are otherwise contaminated by the core field. Our new Curie depth model differs by as much as ±20 km relative to previous models, with the largest differences arising from the low order thermal model and variable susceptibility. Key differences are found in central Africa due to application of a variable susceptibility model, and shield regions, but continents with poor constraints such as Antarctica require additional improvement. This new Curie depth model shows good agreement with continental heat flow observations, and provides further evidence that Curie depth estimates may be used to constrain evaluations of the thermal state of the continental lithosphere, especially in regions with sparse or surface contaminated heat flow observations.

Keywords: Lithospheric thermal state, Geomagnetism, Geomagnetic field, Magnetic susceptibility, Global heat flux

1. Introduction

The thermal state of the lithosphere has implications for a diverse range of processes and physical parameters such as lithospheric strength (e.g. Jiménez-Díaz et al., 2012), can define potential regions of geothermal prospectivity (e.g. Hojat et al., 2016), and the dynamics and stability of ice sheets (e.g. Pattyn, 2010). Heat flow data are often spatially sparse, and are not

*Corresponding author
Email addresses: `matthew.gard@adelaide.edu.au` (M. Gard), `dhasterok@gmail.com` (D. Hasterok)

always representative of the deep crustal thermal state, as heat flow is sensitive to near-surface influences such as hydrothermal circulation, thermal refraction, and the lateral distribution of heat producing elements. Thus, deep thermal crustal constraints derived from temperature-sensitive proxies are not only useful in regions with little to no direct thermal information, but also aid in regions where this heat flow data is available. One way we can produce deep thermal models of the crust and lithosphere is via geophysical proxies such as magnetics.

It is well documented that, in general, there is a relation between surface heat flow and the depth to the bottom of the magnetized layer (e.g. Mayhew, 1982; Okubo and Matsunaga, 1994). As the depth to this layer in the continental crust is generally thermal in origin, this result is not surprising. In this article, we present an updated model for global Curie depths using the equivalent source magnetic dipole (ESMD) method (Dyment and Arkani-Hamed, 1998b) (as previously applied by e.g. Purucker et al., 2002; Fox-Maule et al., 2005, 2009; Hojat et al., 2016). There are four major contributors to the variance between the latest ESMD derived global magnetic crust thickness estimates from Fox-Maule et al. (2009) and the model presented here:

1. an improved satellite lithospheric field model (LCS-1, Olsen et al. (2017));
2. utilisation of a hybrid initial magnetic crustal thickness model built from TC1 (Artemieva, 2006), 3SMAC (Nataf and Ricard, 1996), and a Moho depth estimate from Szwillus et al. (2019);
3. the inclusion of the third vector component in the forward model (longitudinal component, ϕ); and
4. the application of a laterally variable magnetic susceptibility model (modified from Purucker et al., 2002; Hemant, 2003).

The global Curie depth solution resolved in this article matches the magnetic field model synthesised at 300 km altitude and shows reasonable correlation with observed surface heat flow. These results provide further evidence that Curie depth estimates are sensitive to the thermal state for large amounts of the continental lithosphere, and can help constrain temperature and heat flow estimates, especially in regions with sparse or surface contaminated heat flow observations.

2. Background

Most of the internal magnetic field of the Earth is generated in the core, with a smaller contribution sourced from induced and remanent magnetization within the crust (see Hulot et al., 2015, and references therein). Although several orders of magnitude weaker when compared to the core field, the magnetic anomalies resulting from the crust can still be identified from satellite magnetic measurements (e.g. Maus et al., 2002, and references therein).

Magnetisation of the crust resulting from the alignment of magnetic dipoles in susceptible rocks by the core field is known as induced magnetization, and depends on the strength of the inducing field, the magnetic susceptibility, and most importantly for this study, the thickness of the magnetized layer (Dyment and Arkani-Hamed, 1998b; Purucker et al., 2002). It is from this induced crustal magnetic signature that the maximum depth of magnetization can be inferred.

Conversely, remanent magnetization is relic permanent magnetization that exists irrespective of a present inducing field (Dyment and Arkani-Hamed, 1998a; Kent et al., 1978). One of the largest examples of remanent magnetism is the magnetic striping along oceanic spreading centres, whereby molten rock cools through its Curie temperature, and the orientation of the Earth's core field at the time of formation is locked in as a permanent magnetic field (e.g. Macdonald and Holcombe, 1978; Le Pichon and Heirtzler, 1968; Ramana et al., 2001). Though also present in the continental crust, its pattern is mostly indiscernible due to large variance in petrology, age and formation conditions and is generally considered to be dominated by the induced field for the majority of continental regions (Maus and Haak, 2002). When locally present, it can often be significantly greater in strength than the induced magnetization and must at least be considered during interpretations (See Thébault, 2010, for a full summary). More extreme examples of such continental remanent magnetisation include the Bangui magnetic anomaly of central Africa (Regan and Marsh, 1982) and the Kursk magnetic Anomaly in western Russia (Taylor and Frawley, 1987).

Above the Curie temperature, magnetic material loses its ferromagnetic properties and becomes functionally non-magnetic (Wasilewski and Mayhew, 1992). The Curie temperature is unique and ranges dramatically for different magnetic minerals. Magnetite is generally considered the dominant magnetic mineral in the crust, and has a Curie temperature of close to 580 ℃ (e.g. Clark and Emerson, 1991; Langel and Hinze, 1998). While the depth to the bottom of magnetisation can be associated with the magnetite Curie isotherm, this is not always the case. The magnetization of mantle rocks are commonly assumed to be relatively low (Wasilewski and Mayhew, 1992). In regions where the Curie isotherm extends past the depth to the bottom of the crust, it thus follows that the depth of magnetization will be largely bounded by this lithological layer rather than thermal constraints (Figure 1). Regions do exist where magnetization may be present in the mantle, such as the production of magnetite through serpentinization at subduction zones (e.g. The Cascadia convergent margin, Blakely et al., 2005), or potentially via diffusive exsolution within both olivine and pyroxene in colder geotherm environments (e.g. the Kamchatka arc, Ferré et al., 2013). The magnitude of expected anomalies discussed in Ferré et al. (2013) are generally below the noise level of satellite magnetic data (Burton-Johnson et al., 2020), however the tectonic history should indeed be considered when interpreting results from these magnetic based methods.

Global Curie depth estimates have been developed through different methodologies, such as the equivalent source magnetic dipole method (e.g. Purucker et al., 2002; Fox-Maule et al., 2009) or via fractal magnetization (e.g. Li et al., 2017) which conducts the inversion for the magnetic signal in the frequency domain. Both methodologies suffer from differing assumptions and limitations: the ESMD method must make assumptions on magnetic susceptibility distributions across continental and oceanic regions, and the fractal process is constrained by other limitations such as selection of window size which has a direct result of maximum resolvable Curie depth and often fixed fractal scaling factors.

3. Method

We utilise the equivalent source magnetic dipole (ESMD) method for estimating the depth to magnetisation. The ESMD method is described in detail by Dyment and Arkani-Hamed (1998b); Fox-Maule et al. (2009). Put simply, the Earth's crust is discretised into a number of approximately equidistant regions, with each region containing a dipole that is representative of the vertical integration of induced magnetization for that crustal volume. An initial magnetic crustal thickness estimate at each of these locations is modified, and consequently the magnetic moment of each dipole, such that a modelled induced magnetic field at some altitude closely resembles an observed magnetic field model.

3.1. Dipole, observation points, and the synthesized 'observed' fields

Dipole positions, $\bar{r}_j$, are selected using an Inverse Snyder Equal-Area Projection Aperture 3 Hexagon discrete global grid (ISEA3H, Sahr et al., 2003). The ISEA3H represents an approximately equidistant grid spacing, thus giving equal weight spatially for the forward modelling procedure. A typical latitude/longitude grid would have higher density of points at the polar regions compared to the equator, and disproportionately bias the forward modelling procedure to over fit these areas. We utilise 21,872 dipoles, with a mean inter-dipole distance of 156 km. Magnetic field data is synthesized at observation points, $\bar{r}_i$, matching the dipole positions but offset in altitude by 300 km. An example of the density of dipole positions for a region around Australia can be seen in Figure 2a.

We utilise the LCS-1 magnetic field model (Olsen et al., 2017), a lithospheric magnetic field model from spherical harmonic degrees 16 to 185. LCS-1 makes use of a substantially larger data set than previous iterations of satellite derived lithospheric field model; it is derived from magnetic gradient data of a combination of the CHAMP and SWARM satellite missions. By using Swarm N-S and E-W gradient data, a significant reduction in variances compared to a CHAMP-only model is possible (Olsen et al., 2017). LCS-1 presents a number of improvements over previous satellite models, not just isolated to the expansion to higher spherical harmonic degrees. The use of gradient data improves signal-to-noise ratio which permits inclusion of data from periods of increased geomagnetic activity and is less correlated in time which enables a higher data sampling rate. Generally large-scale magnetic field contributions are removed through pre-processing using an a priori model and line levelling which also removes part of the lithospheric signal. By using gradient data, Olsen et al. (2017) also removed the necessity to conduct orbit-to-orbit high-pass filtering or line levelling. Additionally, the availability of E-W gradient data from the Swarm satellite data should also assist in noise reduction in the E-W component of the field model in comparison to a CHAMP N-S gradient or field data derived data set (see Figure 6d in Olsen et al. (2017)).

Alternative models such as EMAG2 (Maus et al., 2009), or WDMAM2 (Lesur et al., 2016) provide exceptional magnetic anomaly detail in many continental and oceanic regions, but are built using a range of data sets with differing resolutions, grids, and high variance in detail across different continents. Contrasts in grid spacing and resolution between regions with highquality near-surface data and satellite models can result in artificial structures in the final Curie depth model, and thus we have chosen to utilise a globally consistent resolution satellite model instead. WDMAM2 and LCS-1 show similar anomalies and amplitudes at matching truncation, but in regions where near-surface data is sparse or non-existent the new LCS-1 satellite model provides improvements (Olsen et al., 2017). Additionally, high resolution variations in the lithospheric magnetic signature are unlikely to be derived from deep thermal anomalies, which is the focus of this article.

We compute the three vector components of the 'observed' lithospheric magnetic field of the observation points (i.e., the radial (r), colatitudinal (θ), and longitudinal (ϕ) vector components) at an altitude of 300 km using spherical harmonic degree 16–100. We chose to truncate the model at degree 100 as the level of detail from spherical harmonic degree 100 to 185 was beyond the resolution of our dipole positions, and thus contributed little to the final solution, and additionally saved on computational time.

As discussed in Section 2, only the induced component of the lithospheric magnetisation depends on the thickness of the magnetized layer, and thus we must ideally isolate the induced field from the observed lithospheric magnetic field. To this end, we remove a remanent magnetic field model for the oceans produced by Dyment and Arkani-Hamed (1998a) and Purucker and Dyment (2000). Such a model does not exist for the continents as it's pattern in continental material are much less systematic as discussed above. Our 'observed' lithospheric induced magnetic field model is illustrated in Figure 3.

The inducing field, i.e. Earth's core field, is well described by various magnetic field models. For our purposes we utilise the CHAOS-6 magnetic field model (Finlay et al., 2016) from spherical harmonic degree 1 through 15 (CHAOS-6-x5, epoch 2018.1) and synthesize the induced field at each dipole location following methodology of Dyment and Arkani-Hamed (1998b). We utilise a forward modelling procedure requiring an initial estimate of the magnetic crustal thickness, and improve the high order estimate (spherical harmonic degree 16–100) via iteration.

3.2. Long-wavelength supplement for magnetic crustal thickness

A crude separation of magnetic field sources (e.g., core and lithospheric contribution) at spherical harmonic degrees 15–16 can be accomplished through satellite derived magnetic field models. However, the long-wavelength magnetic crustal field cannot be distinguished from the core field from spherical harmonic degrees 1–15, and is thus set to 0. This limitation necessitates an initial estimate for the magnetic thickness (for spherical harmonic degree 1–15). In our case, we have used a hybrid model of the TC1 thermal model (Artemieva, 2006) for continental regions excluding Antarctica, the thermal model of 3SMAC (Nataf and Ricard, 1996) for the oceans and Antarctic continent. We synthesized a 580 ℃ isotherm from an extrapolation from the TC1 1300 ℃ $1^\circ \times 1^\circ$ model. It is likely, for many regions of the continental crust, that this model will be a sufficiently accurate estimate of the long-wavelength Curie isotherm field. This model is derived from relationships of tectonothermal ages of lithospheric terranes and a compilation of borehole heat flow measurements, as well as supplementation with xenolith P-T array and electrical conductivity data for the upper mantle. As detailed earlier, in general the depth to the bottom of magnetisation can be considered to be the 580 ℃ isotherm or the depth to the Moho, whichever is shallower. Thus the TC1/3SMAC thermal model was modified to be bounded by the Moho depth model of Szwillus et al. (2019) (see Figure 4b for the relative spatial contributions of each model), and the elevations from CRUST1.0 (Laske et al., 2012).

We prefer the TC1 model over the 3SMAC thermal estimate in most continental regions (used in Purucker et al., 2002; Fox-Maule et al., 2005, 2009; Hojat et al., 2016) as the 3SMAC model is a more simple plate thickness/age model applied to the crust. TC1 is systematically warmer than 3SMAC for most of the cratons. Plate thicknesses derived from seismic tomography tend to be larger than estimates produced by xenolith thermobarometry (e.g. Hasterok and Chapman, 2011), which results in shallower Curie depths. On the whole, TC1 is a more robust estimate of the thermal structure, though there are still some poorly constrained areas. For example, the Tibetan plateau is likely a shallower Curie depth than TC1 suggests as evidenced by regionally extensive mid-crustal conductors at approximately 20 km depth (e.g. Sun et al., 2019; Unsworth et al., 2004). Conversely, in the Australian region the Archean Yilgarn and Pilbara Cratons likely exhibit a deeper Curie isotherm depth. However, Canada and North America appear much more in-line with expectations in TC1 as opposed to 3SMAC, as is Siberia, North China and West Africa and the Congo area. Constraints on the thermal estimate for the Antarctic continent are borderline non-existent in the TC1 model. 3SMAC estimates for the Antarctic continent are more in-line with modern estimates of Curie depth (e.g. Martos et al., 2017), but in reality the signature would be far more heterogeneous than

3SMAC depicts. Nevertheless, we have chosen to utilise the 3SMAC model rather than TC1 for Antarctica. We also prefer using thermal models over crustal thickness models (e.g. CRUST1.0, Laske et al. (2012)) as crustal thickness is not necessarily correlated with the Curie isotherm depth.

3.2.1. Magnetic susceptibility

One of the largest assumptions in the ESMD method is the selection of a magnetic susceptibility model. Lithospheric magnetic field anomalies can be the product of variations in magnetic crustal thickness, or petrological variations resulting in changes of magnetic susceptibility (Purucker and Whaler, 2007). In truth, both parameters contribute in varying magnitudes and thus any solution is inherently non-unique. Assumptions of the relative dominance of these two parameters, or the application of assumed distributions or models for one of these parameters to obtain a unique solution is often required (e.g. Purucker et al., 2002; Hemant and Maus, 2005).

Although there is large heterogeneity in magnetic susceptibilities of different rocks, the typical compositions of continental and oceanic regions are largely coincidental, with a minor weighting towards higher susceptibility values for oceanic material due to greater proportions of elements such as iron, magnesium and titanium (Clark and Emerson, 1991). Some studies (e.g. Counil et al., 1991; Purucker et al., 2002; Fox-Maule et al., 2005; Purucker and Ishihara, 2005; Purucker et al., 2007; Fox-Maule et al., 2009; Rajaram et al., 2009; Thébault, 2010; Hojat et al., 2016; Lei et al., 2018; Jiao and Lei, 2019) make an assumption that the average susceptibility for these dipole positions, which are quite coarsely distributed, can be approximated crudely by a single isotropic estimate for continents and oceans. Conversely, other studies indicate lateral variations in magnetic susceptibility are significant to the lithospheric magnetic field signature and should not be estimated with isotropic estimates. One such model of crustal magnetic susceptibility is that of Hemant (2003), which generated a vertically integrated magnetic susceptibility model based on seismic data, rock samples and geological domain maps. The approach of Hemant (2003) has a number of attractive features, and accounts for some of the magnetic features that are clearly not correlated with magnetic crustal thickness that a simple continental/oceanic model does not (Thébault and Vervelidou, 2015) (notable examples include regions of central Africa).

Nevertheless, the model of Hemant (2003) still contains a large number of broadband assumptions, and under-predicts the magnitude of a number of anomalies (Thébault et al., 2009). Thébault et al. (2009) suggest other world susceptibility distributions such as Purucker et al. (2002), may lead to their predictions falling within expected bounds of magnitudes for continents and oceanic anomalies, but that the Hemant and Maus (2005) model is a far better spatially variable estimate, and closer matches predicted magnetic field features. Thus, we seek a compromise whereby we use the mean continental and oceanic estimates akin to those often used in literature (e.g. Counil et al., 1991; Purucker et al., 2002; Fox-Maule et al., 2005; Purucker and Ishihara, 2005; Purucker et al., 2007; Fox-Maule et al., 2009; Rajaram et al., 2009; Thébault, 2010; Hojat et al., 2016; Lei et al., 2018; Jiao and Lei, 2019), but with the variation model from Hemant (2003) for the continents and oceans applied around this (Figure 5). We delineate oceanic and continental regions by the masking of continental borders in conjunction with bathymetry shallower than 800 m from ETOPO2 (National Geophysical Data Center, 2006). This spatially variable susceptibility model will ideally dampen the influence of magnetic susceptibility on the result such that remaining variations are dominantly a function of magnetic crustal thickness. The susceptibility model used here was generated from the vertically integrated susceptibility model (VIS) of Hemant (2003), divided by the crustal thickness model of 3SMAC (Nataf and Ricard, 1996). We find this susceptibility model produces satisfactory results, and permits crude interpretation of variances between different geological provinces due to magnetic susceptibility.

Vertical variations in magnetic susceptibility are not considered, as these likely only influence very small horizontal scales i.e. above spherical harmonic degree 650 (Langel and Hinze, 1998; Thébault and Vervelidou, 2015). Sedimentary basins were additionally not considered as a source of magnetisation (i.e. magnetic susceptibility set to 0).

3.3. Forward modelling of the magnetic thickness

From an initial magnetic crustal thickness estimate, the magnetic moment of each dipole is calculated, which in turn is used to synthesize a model for the vector components of induced magnetism (following the method of Dyment and Arkani-Hamed (1998b)).

From the initial magnetic crustal thickness model, the magnetic moment of each dipole is calculated which is used to synthesize the vector components of the model of induced magnetism as a result of these magnetization depths (following the method of Dyment and Arkani-Hamed (1998b)). A spherical harmonic expansion of the synthesized induced field from the dipoles is made, and the terms below degree 16 are set to 0 to high-pass filter the magnetization model. The modelled induced magnetic field from the magnetic crustal thickness estimate is then compared to the 'observed' induced magnetic field model (LCS-1, with the oceanic remanent field model removed). If the difference between the modelled and observed magnetic field vector components is larger than a specified tolerance, an adjustment to the previous magnetic crustal thickness estimate is applied.

$$\Delta \bar{\mathbf{B}} = \bar{\mathbf{B}}_{\mathbf{obs}} - \bar{\mathbf{B}}_{\mathbf{model}} \tag{1}$$

$$\Delta \bar{\mathbf{B}} = \mathbf{G} \Delta \mathbf{m_j} \tag{2}$$

where $\bar{\mathbf{B}}_{\mathbf{obs}}$ is the lithospheric magnetic field model (Figure 3), $\bar{\mathbf{B}}_{\mathbf{model}}$ is the magnetic field produced by the magnetic crustal thickness estimate, $\mathbf{G}$ is a matrix related to the negative gradient of the magnetic potential of the dipole located at the observation points (see Fox-Maule et al. (2009)), and $\mathbf{m_j}$ is the magnetic moment of a dipole at observation point r_j.

Rather than constructing a $\mathbf{G}$ matrix that constitutes the influence of the entire set of global dipoles, we use a sparse version of the $\mathbf{G}$ matrix whereby only dipoles within a 2500 km radius are considered (Figure 2a) (See equations in Dyment and Arkani-Hamed, 1998b; Fox-Maule et al., 2009). This sparse matrix reduces the computational resources significantly, and dipoles outside a 2,500 km radius of the observation point are not major contributors to the magnetic field observed. We solve the system of linear equations using the conjugate gradient least-squares method. $\Delta \mathbf{h_j}$, which is directly proportional to $\Delta \mathbf{m_j}$ (See Fox-Maule et al., 2009, for equations), is then added directly to the previous estimate of $\mathbf{h_j}$, where $\mathbf{h_j}$ represents the estimated Curie depth. The process is repeated until the difference between the observed and modelled induced magnetic field vectors converges to within a specified tolerance; in our case, when the root mean square error for each vector component is below 0.05 nT. This tolerance was selected as it represents the energy carried by spherical harmonic degree 100 of the lithospheric field model, and more extensive iterations to refine the model beyond this point did not produce large improvements in the model and began to over-fit and amplify noise.

4. Global Curie depth model

Our updated magnetic crustal thickness model is presented in Figure 6a. We have recreated the model of Fox-Maule et al. (2009) using the MF5/CHAOS1 magnetic field model, two vector components (radial and co-latitudinal), and the initial magnetic crustal thickness derived from the crustal thickness and thermal estimates from 3SMAC (Nataf and Ricard, 1996) for comparison (Figure 7a). The differences between our preferred model and the model of Fox-Maule et al. (2009) can be seen in Figure 6b. These variations can be significant, with a number of continental areas exhibiting differences on the order of ± 20 km.

There are four major contributors to the variance between the previous model of Fox-Maule et al. (2009) and the model presented here:

1. Improvements due to utilisation of a newer satellite field model (LCS1, Olsen et al. (2017));
2. Variance due to a different initial magnetic crustal thickness model (and subsequently the inclusion of it's long-wavelength values in the final model);
3. the inclusion of the third vector component (ϕ); and
4. application of a variable magnetic susceptibility model.

The largest contribution to the long-wavelength difference between our new model and the model of Fox-Maule et al. (2009) is due to the difference in long-wavelength Curie depth estimate. As discussed in Section 3.1, magnetic field models permit the crude separation of the core and lithospheric magnetic field sources, but the long-wavelength magnetic crustal field cannot be distinguished from the core field from spherical harmonic degrees 1–15, thus requiring an estimate from an additional source. Here we have utilised the hybrid TC1 thermal model of Artemieva (2006) and 3SMAC (Nataf and Ricard, 1996), bounded by the Moho estimates of Szwillus et al. (2019) as described in Section 3.2. Figure 4c depicts the low order contribution that remains in our final Curie depth model from the initial estimate, and Figure 8c the difference between the 3SMAC thermally bounded estimate used in Fox-Maule et al. (2009) at these same spherical harmonic degrees. It can clearly be observed that this long-wavelength difference is present in the final model, with largest variance in North America, eastern south America and China (Figure 6b).

The influence of the magnetic susceptibility model applied is also of large significance; it's fingerprint evident in the final model (Figure 6b). Sharp contrasts in susceptibility estimates, such as central Africa and offshore Greenland (Figure 5a), are clearly visible in the final Curie depth estimates with variations. The Curie depth variations due to the spatially variable susceptibility model as opposed to the constant oceanic and continental values selected by Fox-Maule et al. (2009) are depicted in Figure 8d. The susceptibility model applied has dampened a number of sharp contrasts once associated with magnetic crustal thickness in Fox-Maule et al. (2009), particularly in central Africa.

Non-trivial improvements are also observed through utilisation of the LCS-1 magnetic field model as opposed to MF5. Suspicious stripes are present in the comparison figures of Figures 6c and 8a. These are present irrespective of inclusion of the E-W component in the modelling solution, and we suggest these are artefacts present in the MF5 magnetic model due to along-track noise, improved upon in LCS-1. This led to some anomalies presenting as more N-S trending in the previous Curie depth solution using this methodology in the previous global model of Fox-Maule et al. (2009).

To a lesser degree, enhancements have also been gained by utilising the longitudinal (ϕ) component of the magnetic field. This improvement contributes around 3.5% variation (1σ) on average globally between the two and three component solution (Figure 8b). Regions where one of the other components are zero show the most improvement due to the extra vector constraint. Additionally, minor oscillations observed along the magnetic equator in (Fox-Maule et al., 2009) appears to have been minimised further.

4.1. Comparison of Curie depth and heat flow

As the Curie depth is thermal in origin for large swathes of the continental crust, it is reasonable to expect a crude relationship between Curie depth estimates and measured heat flow. In Figure 9, we average the observed continental heat flow compilation from Lucazeau (2019) within each dipole surface area. These heat flow values are directly compared to the Curie depth estimate for continental regions (Figure 10a). Isotherms are constructed using exponentially decreasing heat production with a scale depth of 8 km, and varying thermal parameters to simulate crudely the expected natural scatter for continental regions.

Obviously this comparison has a significant degree of variance. Thermal parameters such as heat production and thermal conductivity are able to vary significantly as depicted in Figure 10, but other near surface influences such as hydrothermal circulation, poor spatial sampling of heat flow, variances in the assumed parameters of the Curie depth modelling procedure, regions of lithologically bounded depth to magnetisation vs thermally controlled etc. all add to the observed scatter of the fit. Nevertheless, we show good agreement with the expected shape of average correlation between heat flow and Curie depth estimates (Figure 10a). We also show a tighter clustering of the Curie depth-heat flow estimates of the previous ESMD derived global Curie depth model of Fox-Maule et al. (2009) (Figure 10b).

An alternative global Curie depth model is also compared; the fractal magnetization model by Li et al. (2017) (Figure 7b). Li et al. (2017) show an excellent correlation to oceanic age, topography, and mid-ocean ridges, more-so than our Curie estimate where this information is not entirely clear. However, the average magnitude of their Curie depth estimates for the oceans are generally in excess of oceanic crustal thickness estimates. There is also a systematic difference in magnitude of Curie depth's across the globe, with those derived from the ESMD method in this article, and similarly for Fox-Maule et al. (2009), generally being deeper than the model of Li et al. (2017), and showing markedly higher intensity variations in intra-continental areas.

Unfortunately Li et al. (2017) do not provide an uncertainty estimate and it is hard to assess our variance in relation to their model. While we estimate relatively large uncertainties (Section 4.2), some long-wavelength trends of the Li et al. (2017) model (Figure 7b) show large anomalies with respect to thermal models and heat flow observations (Figure 9) (e.g. Artemieva, 2006; Lucazeau, 2019). Some stark examples include South-East Africa and Western Australia where heat flow is quite low, but the Curie depth estimate for both of these locations is very shallow. Conversely, Eastern Australia is markedly warmer than Western Australia from the heat flow data. Additionally Eastern South America, Ontario and Quebec in Canada, much of Europe including Germany, and Russia show seemingly better correlations with observed heat flow data.

The most obvious explanation for such stark mean variations between the ESMD method and the method of Li et al. (2017) is that our long-wavelength supplement model may perhaps account for the systematic variation, despite being well correlated with estimates from heat flow and thermal models such as 3SMAC and TC1. Thus, we have also compared just the higher frequency variations of Li et al. (2017) and our model (Figure 11a and b, respectively). While our model shows higher intensity variations at these shorter wavelengths, we also observe a number of similar features with that of Li et al. (2017). For example, south-eastern Africa is much similar than the long-wavelength comparison, and North America shows similar perturbations across the continent. However, many regions still exist with stark variations including Australia, Antarctica and Germany that are clearly not just a simple by-product of the long-wavelength supplement model.

4.2. Deficiencies, uncertainty estimates, and future work

As we have utilised a lithospheric field model, any uncertainties in its derivation propagate directly into the uncertainty of our Curie depth estimate. Assuming comparisons of models produced via different lithospheric field models is an indicator of uncertainty; we observe variance (1σ) of 5.82%, 10.55%, 11.37% respectively when utilising the lithospheric field models MF7, WDMAM and LCS-1. We suggest the use of a more conservative estimate of 15%, and this additionally is more in-line with previous discussions of lithospheric field model uncertainties (Lowes and Olsen, 2004; Fox-Maule et al., 2009).

While we have removed a remanent magnetic field model for the oceans, we have not done so for the continents as no reliable model currently exists. Where applicable, this remanent magnetism may have significant influence on the lithospheric magnetic field observed. Some studies indicate that the majority of magnetic lithospheric field anomalies globally can likely be attributed to induced rather than remanent magnetism in the continents (Counil et al., 1991; Maus and Haak, 2002). Quantifying the uncertainty due to this parameter is rather ambiguous, so we defer to previous estimates of uncertainty related to continental remanent magnetism of around 20% (Fox-Maule et al., 2009).

Based on the variance ranges of the Hemant (2003) model for magnetic susceptibility, we observe an uncertainty of $\pm 15.5\%$ for continents and oceans separately. However, we acknowledge that solutions of magnetic crustal thickness vs. magnetic susceptibility are inherently non-unique, and that our final Curie estimate is proportional to the a priori susceptibility model applied. We estimate a more generous upper bound of around 25%, and appreciate that in some regions this can be easily exceeded (See Figure 8d). It is our hope that the variation model modified from Purucker et al. (2002) and Hemant (2003) has helped to at least dampen the effects of susceptibility variations, and appears to be the case from Figure 6a and b.

An initial estimate for the magnetic thickness is required to supplement the long-wavelength (spherical harmonic degree 1–15) of the Curie depth solution. The lowest order terms of our initial magnetic crustal thickness estimate are thus directly transferred to our final result. The contribution to the final magnetic crustal thickness model that will persist through modelling is presented in Figure 4c i.e., spherical harmonic degrees 1–15 of the spherical harmonic expansion of the Moho bounded TC1 model in Figure 4a. As the longest-wavelength solution is controlled entirely as a result of the initial model fed into the process, it constitutes the largest variance. We believe the hybrid model of TC1 (Artemieva, 2006) and 3SMAC (Nataf and Ricard, 1996) constrained by the Moho depths of Szwillus et al. (2019) constitutes a more modern and improved long-wavelength model than the 3SMAC estimate alone, which has fallen out of favour in recent years in some seismic studies (e.g. Xing and Beghein, 2015). That being said, regions still exist where this combined model appears to not perform well; the Antarctic continent being a notable example. Uncertainty in the long-wavelength model is directly translated into the final Curie solution. While the Moho uncertainty in general is relatively low for many of the higher resolution continental regions (4 km), TC1 constitutes over 66% of the continental long-wavelength solutions. 3SMAC and TC1 differ on the order of $\pm 10.5\%$ (1σ) for continental regions, and we suggest this gives an indication of the uncertainty in the long-wavelength model. Fox-Maule et al. (2009) estimate an uncertainty on the order of 7% due to the initial long-wavelength mode, but this seems too small given the variance between 3SMAC and TC1.

Although we have produced an absolute value for Curie depth in this article, it is proposed that the short-wavelength solutions which are ultimately the target of the modelling process presented here are the most applicable result (Figure 11c). Employing the high-wavelength solutions of magnetic crustal thickness in conjunction with independent long-wavelength estimates of the thermal state of the crust, for example thermal isostasy or seismic tomography, may yield a more holistic thermal result. Additionally, utilising other data sets such as geochemistry may assist in restricting thermal parameters to more appropriate regional values if wanting to estimate heat flow from these Curie depth solutions. The variance about expected generalised heat flow-Curie depth relationship depicted in Figure 10b is the result of many factors, including Curie depth estimation uncertainty, potential existence of meaningful continental remanence, major lithological variations, and regions where the depth to the bottom of magnetisation may not correlate with the Curie isotherm at all, such as at depths below the Moho or where lithological boundaries define sharp contrasts in magnetisation. Such models are the focus of future work. Despite all this, our modelling produces a magnetic crustal thickness estimate that is consistent with the lithospheric magnetic anomalies of the magnetic field model LCS-1, as well as providing a reasonable fit to expected thermal correlations.

Work to reconcile large variations in mean magnetic crustal thickness between different methodologies must be addressed. It is unclear why the model of Li et al. (2017) and the methodology of Purucker et al. (2002) can produce such large variations in mean magnetic crustal thickness. The methodology of Li et al. (2017) seems to resolve spatial variations in the oceans well in regard to age and spreading rate expectations, but some regions of the continents show some very questionable Curie estimates when compared to heat flow data. By removing the long-wavelength supplement field from our model it appears to reduce variations between the model we have presented here and the model of Li et al. (2017) for some regions such as North America, but regions such as Australia still show stark contrasts.

As a result of the high degree of variance in thermal parameters we have decided that the calculation of a global heat flow model is beyond the scope of this article. While studies of global heat loss may justify a need for globally averaged thermal parameters, care must be taken when utilising the results of these studies for localised regions. Heat production can vary significantly on very small spatial scales (Hasterok and Webb, 2017; Gard et al., 2019b,a; Hasterok et al., 2018), and lead to dramatically different heat flow estimates for the same Curie depth estimate. Thus for localised heat flow estimates, it is highly suggested that other data sets be utilised to help constrain these parameters. For example, geochemical sample properties, basement geology knowledge, existing heat flow measurements, temperature profiles, and other geophysical proxies may be used to constrain temperature such as seismic velocity and thermal isostasy. This will be explored in a future study.

5. Concluding remarks

We have produced an updated global Curie depth estimate utilising the equivalent source magnetic dipole (Purucker et al., 2002; Fox-Maule et al., 2009). Results show variations up to ±20 km in contrast to the previous global estimate derived via ESMD methods by Fox-Maule et al. (2009). Utilisation of a hybrid initial magnetic crustal thickness model built from TC1 (Artemieva, 2006), 3SMAC (Nataf and Ricard, 1996), and a Moho depth estimate from Szwillus et al. (2019), as well as the laterally variable magnetic susceptibility model modified from Hemant (2003) and Purucker et al. (2002) dominate the variations. Differences are also associated with the improved satellite lithospheric field model (LCS-1, Olsen et al. (2017)) which refined along track noise present in the previous iterations of this method, as well as the inclusion of the third vector component in the forward model. Regions such as central Africa show the most improvement due to application of the variable susceptibility model, but continents with poor constraints such as Antarctica require further work. Curie depth estimations share a crude pattern to the previous iteration of Fox-Maule et al. (2009), but show large differences in the mean estimates with respect to the fractal methods of Li et al. (2017). The results of this article match both the LCS-1 lithospheric magnetic field model at 300 km altitude, as well as being consistent with observed surface heat flow. This model provides further evidence that Curie depth estimates are sensitive to the thermal state for large amounts of the continental lithosphere, and may be used to help constrain temperature and heat flow estimates, especially in regions with sparse or surface contaminated heat flow observations.

6. Acknowledgements

We would like to thank Liejun Wang for his comments on the article, and two anonymous reviewers for their comprehensive suggestions that markedly improved the article structure. A number of scripts were adapted from codes from Simons and Dahlen (2006), and Frederik Simons provided helpful communications. Additionally, thank you to Azadeh Hojat, Bernhard Steinberger and Nils Olsen for providing assistance with data sets. The support of Geoscience Australia is gratefully acknowledged.

M. Gard was supported by an Australian Government Research Training Program Scholarship. This research was supported partially by the Australian Government through the Australian Research Council's Discovery Projects funding scheme (project DP180104074).

References

Artemieva, I.M., 2006. Global 1x1 thermal model TC1 for the continental lithosphere: Implications for lithosphere secular evolution. Tectonophysics 416, 245 – 277. URL: http://www.sciencedirect.com/science/article/pii/S0040195105006256, doi:10.1016/j.tecto.2005.11.022. the Heterogeneous Mantle.

Blakely, R.J., Brocher, T.M., Wells, R.E., 2005. Subduction-zone magnetic anomalies and implications for hydrated forearc mantle. Geology 33, 445–448. URL: http://pubs.er.usgs.gov/publication/70029340, doi:10.1130/G21447.1.

Burton-Johnson, A., Dziadek, R., Martin, C., 2020. Geothermal heat flow in Antarctica: current and future directions. The Cryosphere Discussions 2020, 1–45. URL: https://www.the-cryosphere-discuss.net/tc-2020-59/, doi:10.5194/tc-2020-59.

Clark, D.A., Emerson, J.B., 1991. Notes on rock magnetization characteristics in applied geophysical studies. Exploration Geophysics 22, 547–555. doi:10.1071/EG991547.

Counil, J.L., Cohen, Y., Achache, J., 1991. The global continent-ocean magnetization contrast. Earth and Planetary Science Letters 103, 354 – 364. doi:10.1016/0012-821X(91)90172-E.

Dyment, J., Arkani-Hamed, J., 1998a. Contribution of lithospheric remanent magnetization to satellite magnetic anomalies over the world's oceans. Journal of Geophysical Research: Solid Earth 103, 15423–15441. URL: https://agupubs.onlinelibrary.wiley.com/doi/abs/10.1029/97JB03574, doi:10.1029/97JB03574.

Dyment, J., Arkani-Hamed, J., 1998b. Equivalent source magnetic dipoles revisited. Geophysical Research Letters 25, 2003–2006. URL: https://agupubs.onlinelibrary.wiley.com/doi/abs/10.1029/98GL51331, doi:10.1029/98GL51331, arXiv:https://agupubs.onlinelibrary.wiley.com/doi/pdf/10.1029/98GL51331.

Ferré, E.C., Friedman, S.A., Martín-Hernández, F., Feinberg, J.M., Conder, J.A., Ionov, D.A., 2013. The magnetism of mantle xenoliths and potential implications for sub-Moho magnetic sources. Geophysical Research Letters 40, 105–110. URL: https://agupubs.onlinelibrary.

wiley.com/doi/abs/10.1029/2012GL054100, doi:10.1029/2012GL054100, arXiv:https://agupubs.onlinelibrary.wiley.com/doi/pdf/10.1029/2012GL054100.

Finlay, C.C., Olsen, N., Kotsiaros, S., Gillet, N., Tøffner-Clausen, L., 2016. "recent geomagnetic secular variation from swarm and ground observatories as estimated in the chaos-6 geomagnetic field model". Earth, Planets and Space 68, 112. doi:10.1186/s40623-016-0486-1.

Fox-Maule, C., Purucker, M.E., Olsen, N., 2009. Inferring Magnetic Crustal Thickness and Geothermal Heat Flux from Crustal Magnetic Field Models. URL: http://core2.gsfc.nasa.gov/research/purucker/foxmaule_dkc09-09_greenland.pdf.

Fox-Maule, C., Purucker, M.E., Olsen, N., Mosegaard, K., 2005. Heat Flux Anomalies in Antarctica Revealed by Satellite Magnetic Data. Science 309, 464–467. URL: https://science.sciencemag.org/content/309/5733/464, doi:10.1126/science.1106888, arXiv:https://science.sciencemag.org/content/309/5733/464.full.pdf.

Gard, M., Hasterok, D., Halpin, J.A., 2019a. Global whole-rock geochemical database compilation. Earth System Science Data 11, 1553–1566. URL: https://essd.copernicus.org/articles/11/1553/2019/, doi:10.5194/essd-11-1553-2019.

Gard, M., Hasterok, D., Hand, M., Cox, G., 2019b. Variations in continental heat production from 4 Ga to the present: Evidence from geochemical data. Lithos 342–343, 391–406. URL: http://www.sciencedirect.com/science/article/pii/S0024493719302245, doi:10.1016/j.lithos.2019.05.034.

Hasterok, D., Chapman, D., 2011. Heat production and geotherms for the continental lithosphere. Earth and Planetary Science Letters 307, 59 – 70. doi:10.1016/j.epsl.2011.04.034.

Hasterok, D., Gard, M., Webb, J., 2018. On the radiogenic heat production of metamorphic, igneous, and sedimentary rocks. Geoscience Frontiers 9, 1777 – 1794. URL: http://www.sciencedirect.com/science/article/pii/S1674987117301937, doi:https://doi.org/10.1016/j.gsf.2017.10.012. "Reliability Analysis of Geotechnical Infrastructures".

Hasterok, D., Webb, J., 2017. On the radiogenic heat production of igneous rocks. Geoscience Frontiers 8, 919 – 940. URL: http://www.sciencedirect.com/science/article/pii/S1674987117300579, doi:10.1016/j.gsf.2017.03.006.

Hemant, K., 2003. Modeling and interpretation of global lithospheric magnetic anomalies. Ph.D. thesis. Freien Universität.

Hemant, K., Maus, S., 2005. Geological modeling of the new CHAMP magnetic anomaly maps using a geographical information system technique. Journal of Geophysical Research: Solid Earth 110. doi:10.1029/2005JB003837.

Hojat, A., Fox-Maule, C., Singh, K.H., 2016. Reconnaissance exploration of potential geothermal sites in Kerman province, using Curie depth calculations. Journal of the Earth and Space Physics 41, 95–104. doi:10.22059/JESPHYS.2015.57226.

Hulot, G., Sabaka, T., Olsen, N., Fournier, A., 2015. 5.02 - The present and future geomagnetic field, in: Schubert, G. (Ed.), Treatise on Geophysics (Second Edition). second edition ed.. Elsevier, Oxford, pp. 33 – 78. doi:10.1016/B978-0-444-53802-4.00096-8.

Jiao, L., Lei, Y., 2019. Curie point depth inversion and its potential application to geothermal resource exploration. pp. 193–196. doi:10.1190/GEM2019-049.1.

Jiménez-Díaz, A., Ruiz, J., Villaseca, C., Tejero, R., Capote, R., 2012. The thermal state and strength of the lithosphere in the Spanish Central System and Tajo Basin from crustal heat production and thermal isostasy. Journal of Geodynamics 58, 29 – 37. doi:10.1016/j.jog.2012.01.005.

Kent, D.V., Honnorez, B.M., Opdyke, N.D., Fox, P.J., 1978. Magnetic properties of dredged oceanic gabbros and the source of marine magnetic anomalies. Geophysical Journal International 55, 513–537. doi:10.1111/j.1365-246X.1978.tb05925.x.

Langel, R.A., Hinze, W.J., 1998. The Magnetic Field of the Earth's Lithosphere: The Satellite Perspective. Cambridge University Press. doi:10.1017/CBO9780511629549.

Laske, G., Masters, G., Ma, Z., Pasyanos, M.E., 2012. CRUST1.0: An Updated Global Model of Earth's Crust, in: EGU General Assembly Conference Abstracts, p. 3743.

Le Pichon, X., Heirtzler, J.R., 1968. Magnetic anomalies in the indian ocean and sea-floor spreading. Journal of Geophysical Research (1896-1977) 73, 2101–2117. doi:10.1029/JB073i006p02101.

Lei, Y., Jiao, L., Chen, H., 2018. Possible correlation between the vertical component of lithospheric magnetic field and continental seismicity. Earth, Planets and Space 70, 179. doi:10.1186/s40623-018-0949-7.

Lesur, V., Hamoudi, M., Choi, Y., Dyment, J., Thébault, E., 2016. Building the second version of the World Digital Magnetic Anomaly Map (WDMAM). Earth, Planets and Space 68, 27. doi:10.1186/s40623-016-0404-6.

Li, C.F., Lu, Y., Wang, J., 2017. A global reference model of Curie-point depths based on EMAG2. Scientific Reports 7, 45129. doi:10.1038/srep45129.

Lowes, F.J., Olsen, N., 2004. A more realistic estimate of the variances and systematic errors in spherical harmonic geomagnetic field models. Geophysical Journal International 157, 1027–1044. doi:10.1111/j.1365-246X.2004.02256.x.

Lucazeau, F., 2019. Analysis and mapping of an updated terrestrial heat flow data set. Geochemistry, Geophysics, Geosystems 20, 4001–4024. URL: https://agupubs.onlinelibrary.wiley.com/doi/abs/10.1029/2019GC008389, doi:10.1029/2019GC008389, arXiv:https://agupubs.onlinelibrary.wiley.com/doi/pdf/10.1029/2019GC008389.

Macdonald, K.C., Holcombe, T., 1978. Inversion of magnetic anomalies and sea-floor spreading in the cayman trough. Earth and Planetary Science Letters 40, 407 – 414. doi:10.1016/0012-821X(78)90163-2.

Martos, Y.M., Catalán, M., Jordan, T.A., Golynsky, A., Golynsky, D., Eagles, G., Vaughan, D.G., 2017. Heat Flux Distribution of Antarctica Unveiled. Geophysical Research Letters 44, 11,417–11,426. URL: https://agupubs.onlinelibrary.wiley.com/doi/abs/10.1002/2017GL075609, doi:10.1002/2017GL075609, arXiv:https://agupubs.onlinelibrary.wiley.com/doi/pdf/10.1002/2017GL075609.

Maus, S., Barckhausen, U., Berkenbosch, H., Bournas, N., Brozena, J., Childers, V., Dostaler, F., Fairhead, J.D., Finn, C., von Frese, R.R.B., Gaina, C., Golynsky, S., Kucks, R., Lühr, H., Milligan, P., Mogren, S., Müller, R.D., Olesen, O., Pilkington, M., Saltus, R., Schreckenberger, B., Thébault, E., Caratori Tontini, F., 2009. Emag2: A 2–arc min resolution earth magnetic anomaly grid compiled from satellite, airborne, and marine magnetic measurements. Geochemistry, Geophysics, Geosystems 10. doi:10.1029/2009GC002471.

Maus, S., Haak, V., 2002. Is the long wavelength crustal magnetic field dominated by induced or by remanent magnetisation? J. Ind. Geophys. Union 6, 1 – 5.

Maus, S., Rother, M., Holme, R., Lühr, H., Olsen, N., Haak, V., 2002. First scalar magnetic anomaly map from champ satellite data indicates weak lithospheric field. Geophysical Research Letters 29, 45–1–47–4. doi:10.1029/2001GL013685.

Mayhew, M.A., 1982. Application of satellite magnetic anomaly data to curie isotherm mapping. Journal of Geophysical Research: Solid Earth 87, 4846–4854. URL: https://agupubs.onlinelibrary.wiley.com/doi/abs/10.1029/JB087iB06p04846, doi:10.1029/JB087iB06p04846, arXiv:https://agupubs.onlinelibrary.wiley.com/doi/pdf/10.1029/JB087iB06p04846.

Nataf, H.C., Ricard, Y., 1996. 3smac: an a priori tomographic model of the upper mantle based on geophysical modeling. Physics of the Earth and Planetary Interiors 95, 101 – 122. URL: http://www.sciencedirect.com/science/article/pii/0031920195031057, doi:10.1016/0031-9201(95)03105-7.

National Geophysical Data Center, 2006. 2-minute Gridded Global Relief Data (ETOPO2) v2. doi:10.7289/V5J1012Q. Accessed 07.07.2020.

Okubo, Y., Matsunaga, T., 1994. Curie point depth in northeast Japan and its correlation with regional thermal structure and seismicity. Journal of Geophysical Research: Solid Earth 99, 22363–22371. URL: https://agupubs.onlinelibrary.wiley.com/doi/abs/10.1029/94JB01336, doi:10.1029/94JB01336, arXiv:https://agupubs.onlinelibrary.wiley.com/doi/pdf/10.1029/94JB01336.

Olsen, N., Ravat, D., Finlay, C.C., Kother, L.K., 2017. LCS-1: a high-resolution global model of the lithospheric magnetic field derived from CHAMP and Swarm satellite observations. Geophysical Journal International 211, 1461–1477. URL: https://doi.org/10.1093/gji/ggx381, doi:10.1093/gji/ggx381, arXiv:https://academic.oup.com/gji/article-pdf/211/3/1461/21308773/ggx381.pdf.

Pattyn, F., 2010. Antarctic subglacial conditions inferred from a hybrid ice sheet/ice stream model. Earth and Planetary Science Letters 295, 451 – 461. URL: http://www.sciencedirect.com/science/article/pii/S0012821X10002712, doi:10.1016/j.epsl.2010.04.025.

Purucker, M., Ishihara, T., 2005. Magnetic images of the Sumatra region crust. Eos, Transactions American Geophysical Union 86, 101–102. URL: https://agupubs.onlinelibrary.wiley.com/doi/abs/10.1029/2005EO100002, doi:10.1029/2005EO100002.

Purucker, M., Langlais, B., Olsen, N., Hulot, G., Mandea, M., 2002. The southern edge of cratonic north america: Evidence from new satellite magnetometer observations. Geophysical Research Letters 29, 56–1–56–4. doi:10.1029/2001GL013645.

Purucker, M., Sabaka, T., Le, G., Slavin, J.A., Strangeway, R.J., Busby, C., 2007. Magnetic field gradients from the st-5 constellation: Improving magnetic and thermal models of the lithosphere. Geophysical Research Letters 34. doi:10.1029/2007GL031739.

Purucker, M., Whaler, K., 2007. 5.06 - crustal magnetism, in: Schubert, G. (Ed.), Treatise on Geophysics. Elsevier, Amsterdam, pp. 195 – 235. doi:10.1016/B978-044452748-6.00091-2.

Purucker, M.E., Dyment, J., 2000. Satellite magnetic anomalies related to seafloor spreading in the South Atlantic Ocean. Geophysical Research Letters 27, 2765–2768. URL: https://agupubs.onlinelibrary.wiley.com/doi/abs/10.1029/1999GL008437, doi:10.1029/1999GL008437, arXiv:https://agupubs.onlinelibrary.wiley.com/doi/pdf/10.1029/1999GL008437.

Rajaram, M., Anand, S., Hemant, K., Purucker, M., 2009. Curie isotherm map of indian subcontinent from satellite and aeromagnetic data. Earth and Planetary Science Letters 281, 147 – 158. doi:10.1016/j.epsl.2009.02.013.

Ramana, M., Ramprasad, T., Desa, M., 2001. Seafloor spreading magnetic anomalies in the Enderby Basin, East Antarctica. Earth and Planetary Science Letters 191, 241 – 255. doi:10.1016/S0012-821X(01)00413-7.

Regan, R.D., Marsh, B.D., 1982. The Bangui Magnetic Anomaly: Its geological origin. Journal of Geophysical Research: Solid Earth 87, 1107–1120. URL: https://agupubs.onlinelibrary.wiley.com/doi/abs/10.1029/JB087iB02p01107, doi:10.1029/JB087iB02p01107, arXiv:https://agupubs.onlinelibrary.wiley.com/doi/pdf/10.1029/JB087iB02p01107.

Sahr, K., White, D., Kimerling, A.J., 2003. Geodesic discrete global grid systems. Cartography and Geographic Information Science 30, 121–134. doi:10.1559/152304003100011090.

Simons, F.J., Dahlen, F.A., 2006. Spherical Slepian functions and the polar gap in geodesy. Geophysical Journal International 166, 1039–1061. URL: https://doi.org/10.1111/j.1365-246X.2006.03065.x, doi:10.1111/j.1365-246X.2006.03065.x, arXiv:https://academic.oup.com/gji/article-pdf/166/3/1039/6098905/166-3-1039.pdf.

Sun, X., Zhan, Y., Zhao, L., Chen, X., Sun, J., Li, C., Cui, T., Han, J., 2019. Electrical structure of the Kunlun–Qinling fault system, northeastern Tibetan Plateau, inferred from 3-D inversion of magnetotelluric data. Journal of Asian Earth Sciences 181, 103910. doi:10.1016/j.jseaes.2019.103910.

Szwillus, W., Afonso, J.C., Ebbing, J., Mooney, W.D., 2019. Global crustal thickness and velocity structure from geostatistical analysis of seismic data. Journal of Geophysical Research: Solid Earth 124, 1626–1652. URL: https://agupubs.onlinelibrary.wiley.com/doi/abs/10.1029/2018JB016593, doi:10.1029/2018JB016593, arXiv:https://agupubs.onlinelibrary.wiley.com/doi/pdf/10.1029/2018JB016593.

Taylor, P.T., Frawley, J.J., 1987. Magsat anomaly data over the kursk region, u.s.s.r. Physics of the Earth and Planetary Interiors 45, 255 – 265. URL: http://www.sciencedirect.com/science/article/pii/0031920187900148, doi:https://doi.org/10.1016/0031-9201(87)90014-8.

Thébault, E., 2010. The magnetic field of the earth's lithosphere. Space Science Reviews 155, 95 – 127. doi:10.1007/s11214-010-9667-6.

Thébault, E., Hemant, K., Hulot, G., Olsen, N., 2009. On the geographical distribution of induced time-varying crustal magnetic fields. Geophysical Research Letters 36. doi:10.1029/2008GL036416.

Thébault, E., Vervelidou, F., 2015. A statistical spatial power spectrum of the Earth's lithospheric magnetic field. Geophysical Journal International 201, 605–620. doi:10.1093/gji/ggu463.

Unsworth, M., Wenbo, W., Jones, A.G., Li, S., Bedrosian, P., Booker, J., Sheng, J., Ming, D., Handong, T., 2004. Crustal and upper mantle structure of northern Tibet imaged with magnetotelluric data. Journal of Geophysical Research: Solid Earth 109. URL: https://agupubs.onlinelibrary.wiley.com/doi/abs/10.1029/2002JB002305, doi:https://doi.org/10.1029/2002JB002305, arXiv:https://agupubs.onlinelibrary.wiley.com/doi/pdf/10.1029/2002JB002305.

Wasilewski, P.J., Mayhew, M.A., 1992. The moho as a magnetic boundary revisited. Geophysical Research Letters 19, 2259–2262. URL: https://agupubs.onlinelibrary.wiley.com/doi/abs/10.1029/92GL01997, doi:10.1029/92GL01997, arXiv:https://agupubs.onlinelibrary.wiley.com/doi/pdf/10.1029/92GL01997.

Xing, Z., Beghein, C., 2015. A Bayesian approach to assess the importance of crustal corrections in global anisotropic surface wave tomography. Geophysical Journal International 203, 1832–1846. doi:10.1093/gji/ggv401, arXiv:https://academic.oup.com/gji/article-pdf/203/3/1832/8036379/ggv401.pdf.

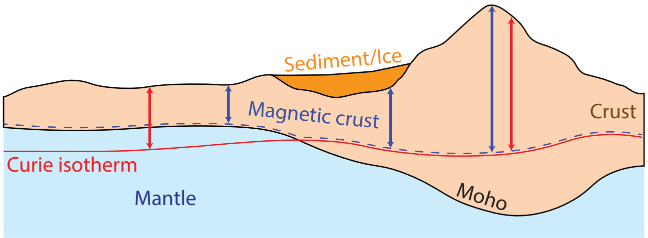

Figure 1: The relationship between Curie depth and the magnetic crust. The depth to magnetisation is generally thermally bounded in regions where the Curie isotherm is shallower than the Moho, and lithologically controlled when not. Sedimentary basins are generally very low in contribution to the magnetic signature and are excluded in this analysis.

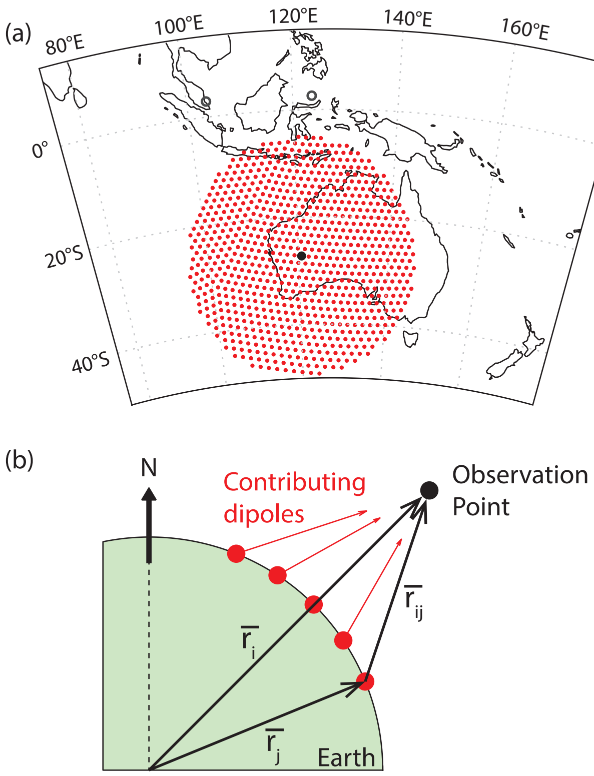

Figure 2: Visual illustration of the computational scheme used to estimate the magnetic field at a point using ESMD. a) Map view of an observation point (black) surrounded by dipole locations (<2500 km) used for the calculation. b) Cross-section showing altitude of observation point relative to dipole locations. $\bar{r}_i$ is the vector from the centre of the Earth to the observation point, $\bar{r}_j$ the vector to the dipole position, and $\bar{r}_{ij}$ the vector between them.

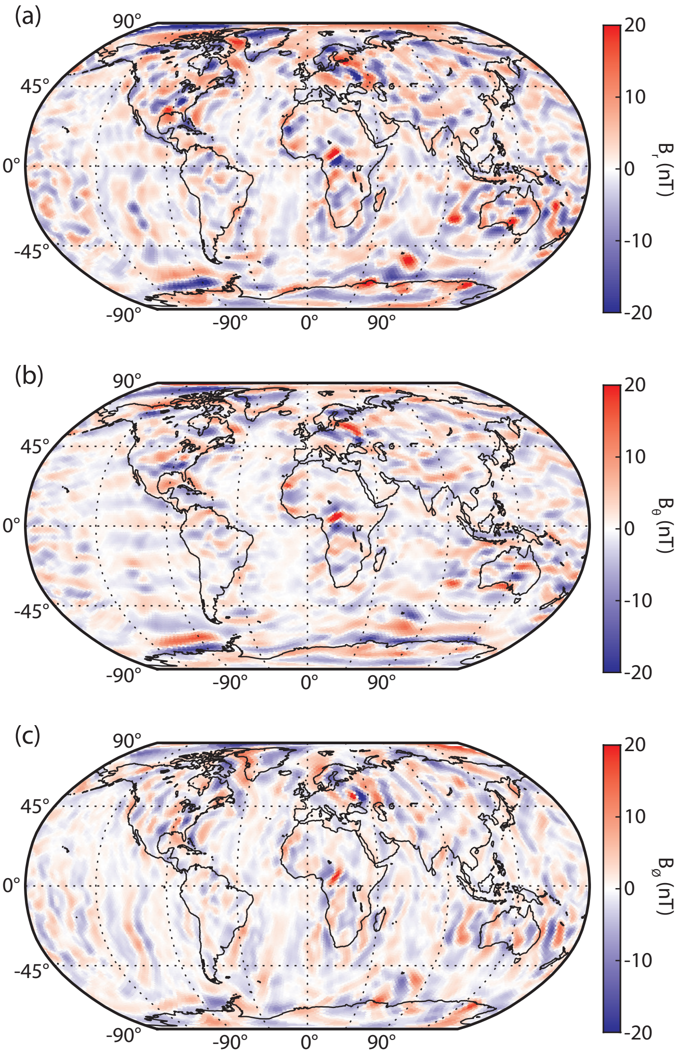

Figure 3: The LCS-1 magnetic field model components with the remanent oceanic field model removed: a) radial component, r; b) colatitudinal component, θ; and c) longitudinal component, ϕ

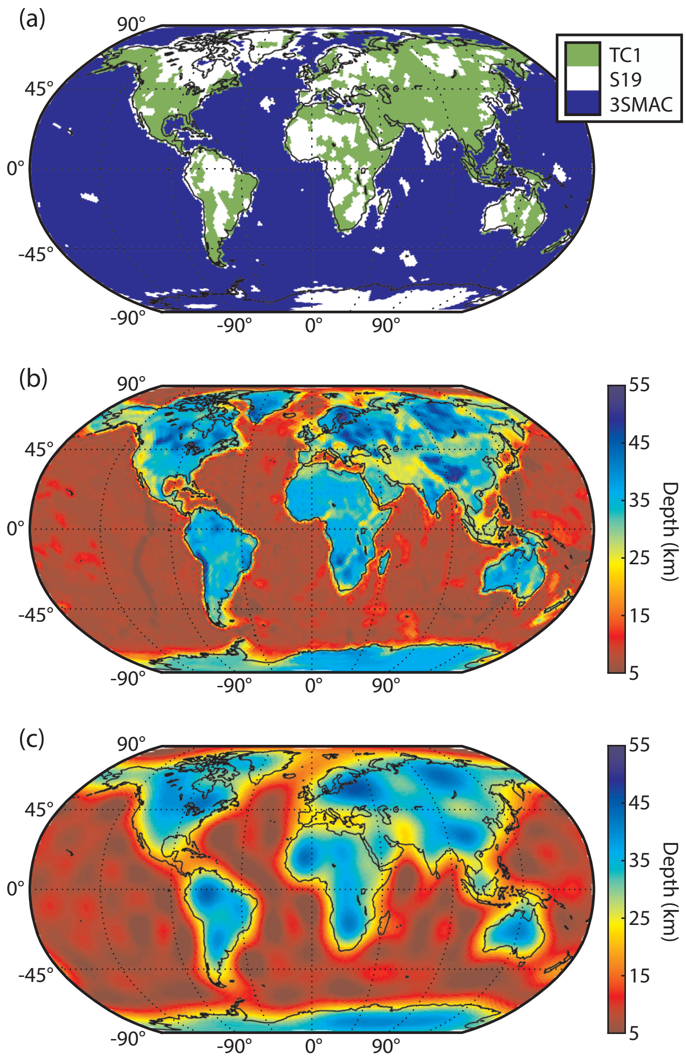

Figure 4: Constructing the spherical harmonic degree 1–15 initial Curie depth supplement model. a) Spatial diagram of the relative contributions from each model. TC1 (Artemieva, 2006)), 3SMAC (Nataf and Ricard, 1996), and S19 (Szwillus et al., 2019), b) TC1/3SMAC thermal model bounded by the Szwillus et al. (2019) Moho depth model, c) Spherical harmonic degrees 1–15 of the model in a).

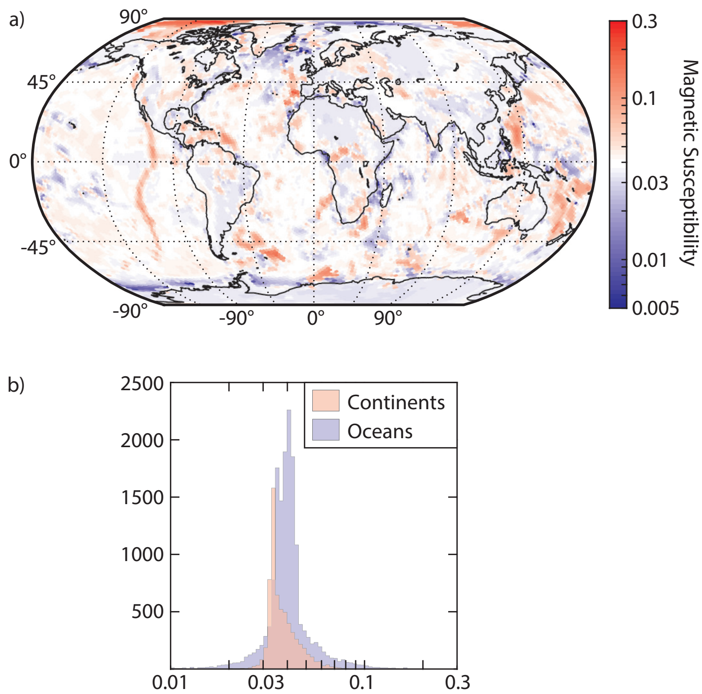

Figure 5: Magnetic susceptibility model utilised, modified from Hemant (2003) and Purucker et al. (2002). a) Spatial distributions. b) Histogram of continental and oceanic susceptibilities.

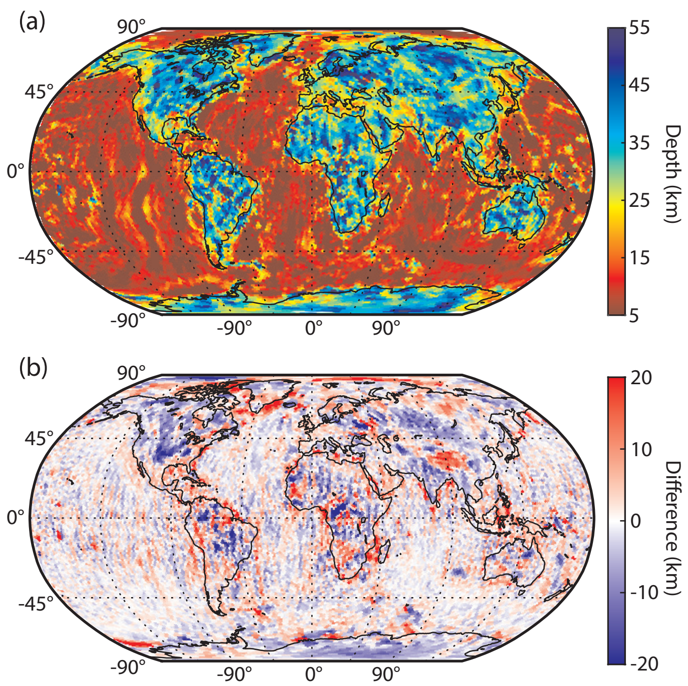

Figure 6: Updated ESMD derived global Curie depth model. a) Curie depth estimate of this article, consistent with the lithospheric magnetic field model LCS-1. b) Difference between the recreation of the Fox-Maule et al. (2009) model in Figure 7a and our model (i.e. subtracting the model of Fox-Maule et al. (2009) from our new model).

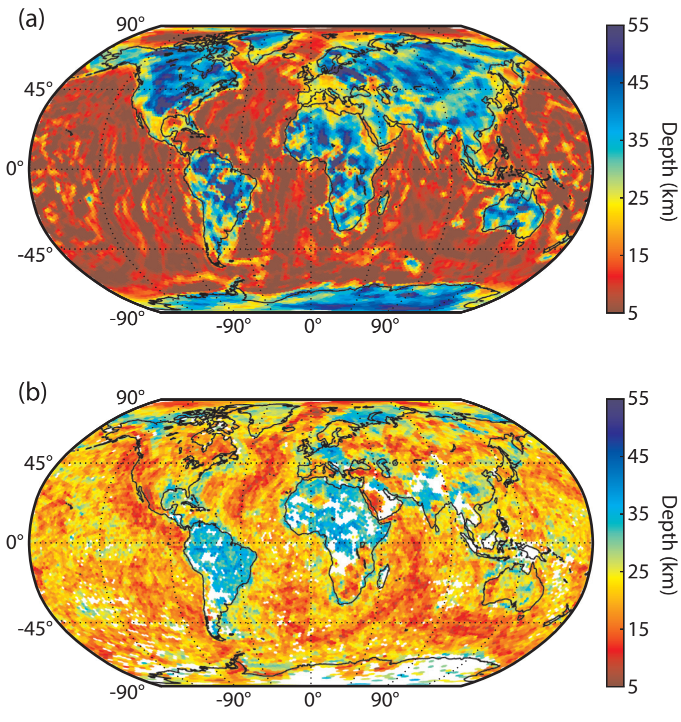

Figure 7: Global Curie depth models. a) Recreation of the Fox-Maule et al. (2009) model. b) Curie depth estimate of Li et al. (2017).

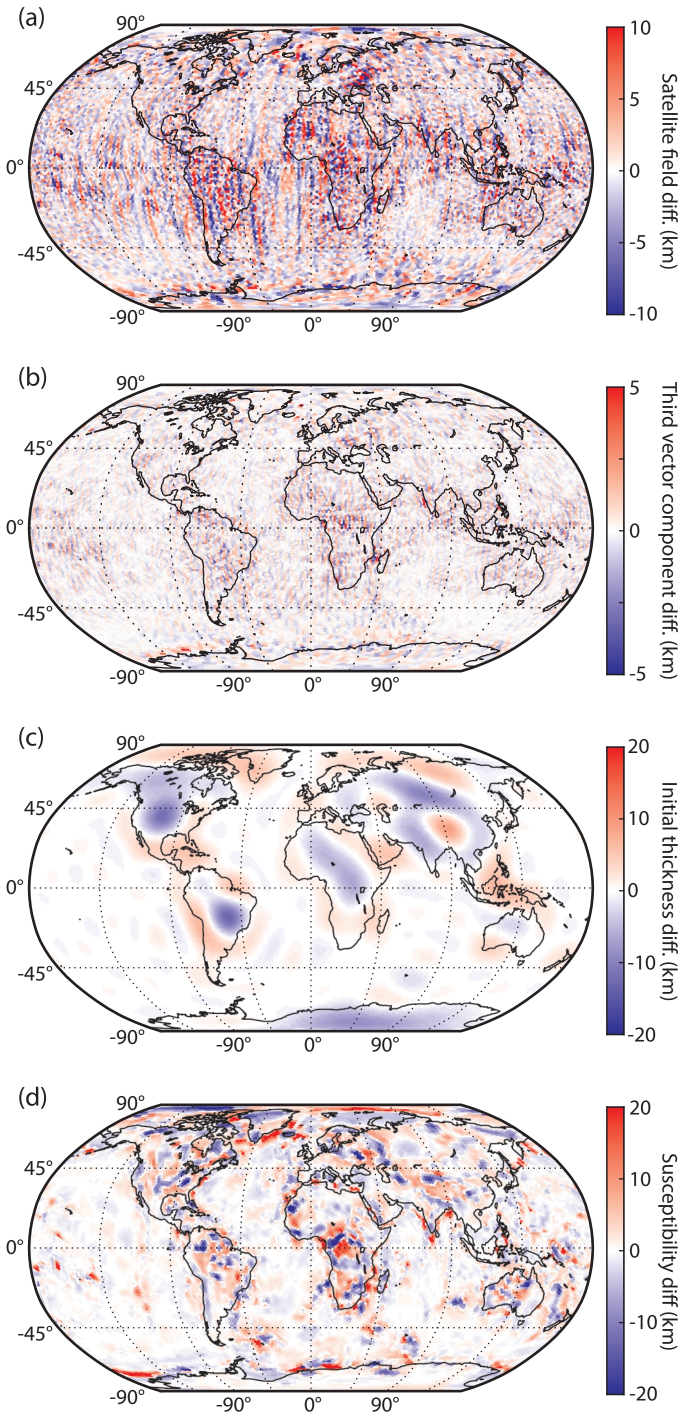

Figure 8: Variations in Curie depth estimate from the previous model of Fox-Maule et al. (2009) as a result of individual parameter changes. a) Differing satellite field model (LCS-1 vs MF5/CHAOS1) b) Two vs. three vector component solution c) Hybrid long-wavelength model of this article vs. 3SMAC only (spherical harmonic degrees 1–15) d) Magnetic susceptibility changes compared to Fox-Maule et al. (2009). A suite of models were calculated varying only one parameter at a time, and all differences are calculated by subtracting the old method from the new.

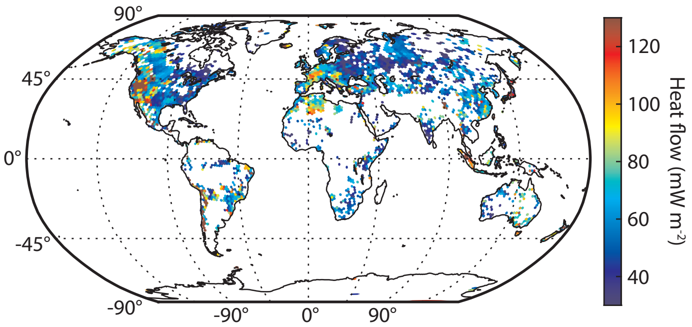

Figure 9: Heat flow data from Lucazeau (2019) averaged within each dipole area.

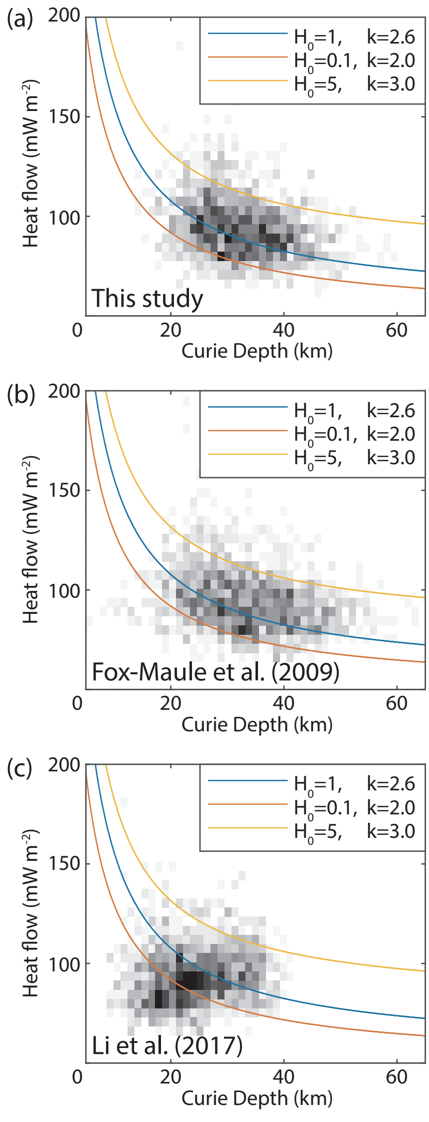

Figure 10: Comparison of Curie depth estimates against measured continental heat flow compilation of Lucazeau (2019). a) This study, b) the model of Fox-Maule et al. (2009), c) the model of Li et al. (2017). Curves in a), b) and c) depict expected heat flow for a Curie depth estimate when assigned simple thermal parameters denoted on graph. Thermal Conductivity (k) applied is constant for the crustal column, and heat production (H_0) denotes the surface heat production with an exponentially decreasing curve with depth, with scale depth of 8 km.

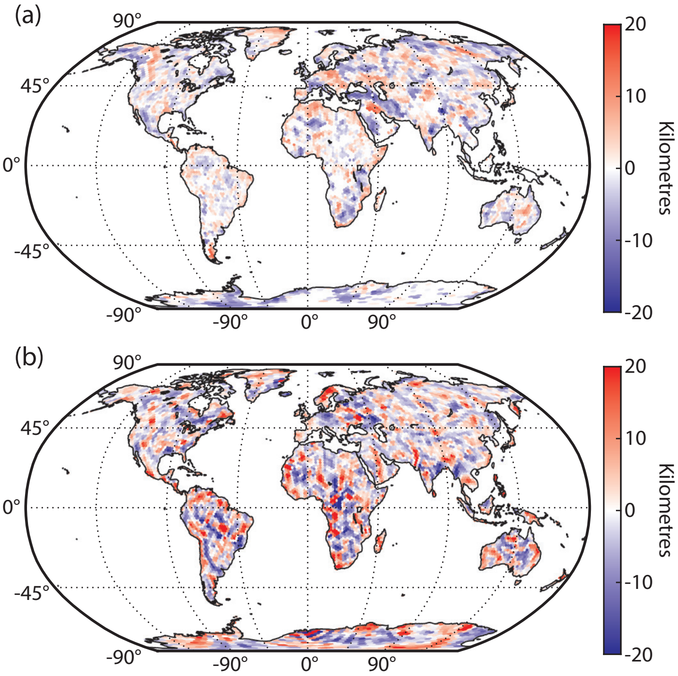

Figure 11: Comparison of only the short wavelength variations of the Curie depth result with Li et al. (2017). a) Li et al. (2017), b) This study.